Available online at www.sciencedirect.com
ScienceDirect
Mendeleev Commun., 2023, **33**, 836–838

Mendeleev Communications

An egg-shell PdAg/α-Al_2O_3 single-atom alloy catalyst for selective acetylene hydrogenation

Pavel V. Markov, Igor S. Mashkovsky,* Galina N. Baeva, Dmitry P. Melnikov and Alexander Yu. Stakheev

N. D. Zelinsky Institute of Organic Chemistry, Russian Academy of Sciences, 119991 Moscow, Russian Federation. Fax: +7 499 135 5328; e-mail: im@ioc.ac.ru

DOI: 10.1016/j.mencom.2023.10.032

The PdAg/α-Al_2O_3 catalyst with an egg-shell distribution of single-atom alloy (SAA) Pd_1Ag nanoparticles was obtained using the complex $PdAg_2(OAc)_4(HOAc)_4$ as a precursor and characterized by FESEM-EDS, XPS, and DRIFTS CO analysis. The egg-shell Pd_1Ag SAA catalyst demonstrated superior selectivity in the hydrogenation of acetylene in acetylene–ethylene feed.

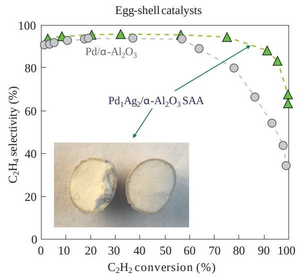

Keywords: acetylene hydrogenation, egg-shell catalyst, single-atom alloy catalyst, PdAg alloy, heterobimetallic complex, catalyst characterization.

The selective hydrogenation of acetylene is of fundamental significance for both the petrochemical industry and laboratory practice.[1–3] In the industry, this reaction serves for purifying ethylene streams obtained after naphtha cracking before polyethylene production to prevent polymerization catalyst poisoning. Palladium-based catalysts are typically used for selective hydrogenation in order to reduce trace amounts of acetylene (0.5–2%) in steam cracking products to a ppm level while minimizing ethylene hydrogenation.[4,5] Monometallic palladium exhibits impressive hydrogenation activity but insufficient selectivity and long-term stability. Modification of Pd with a second metal is an effective way to improve its selectivity.

Recently, excellent performance in the hydrogenation of acetylene and substituted alkynes was observed with single-atom alloy (SAA) catalysts.[6–8] The term SAA was originally proposed in 2012.[9] Typical SAA catalysts are comprised of the single atoms of a catalytically active metal alloyed into the surface of a less reactive or inactive host metal. PdAg SAA catalytic compositions are used in acetylene hydrogenation.[10–15] In these catalysts, the surface structure of single-atom Pd_1 active sites is formed *via* the isolation of active Pd atoms by Ag atoms, which are inactive in hydrogenation providing high target selectivity. However, despite the excellent selectivity of SAA catalysts, their use is currently limited to laboratory applications. In industry, mainly PdAg egg-shell catalysts are implemented for acetylene hydrogenation because their structure favors ethylene desorption from the catalyst surface and prevents its further hydrogenation to ethane maintaining a high target selectivity.[16–21]

In this work, we obtained a novel Pd_1Ag/Al_2O_3 SAA catalyst with the egg-shell distribution of the active component. When preparing a catalyst with uniform PdAg nanoparticles and the SAA structure of active sites, the deposition of Pd and Ag components on the Al_2O_3 surface in close proximity to each other is of great importance. We used the heterobimetallic $PdAg_2(OAc)_4(HOAC)_4$ complex as a precursor of the active component.[22] In this complex, Pd and Ag atoms are strongly linked by acetate bridges to ensure close vicinity between these atoms during catalyst synthesis.[23] The 0.06 wt% Pd−0.12 wt% Ag/Al_2O_3 SAA catalyst was prepared. Monometallic 0.06 wt% Pd/Al_2O_3 catalyst was used as a reference sample. The egg-shell structure was attained by the preliminary acetic acid treatment of parent α-Al_2O_3. The above samples were denoted as Pd_1Ag and Pd, respectively. The samples were characterized by FESEM-EDS, XPS, TEM, and DRIFTS CO (see Online Supplementary Materials for experimental details).

The distribution of Pd and Ag in a catalyst granule was determined using FESEM-EDS. Figure 1 shows the EDS-line

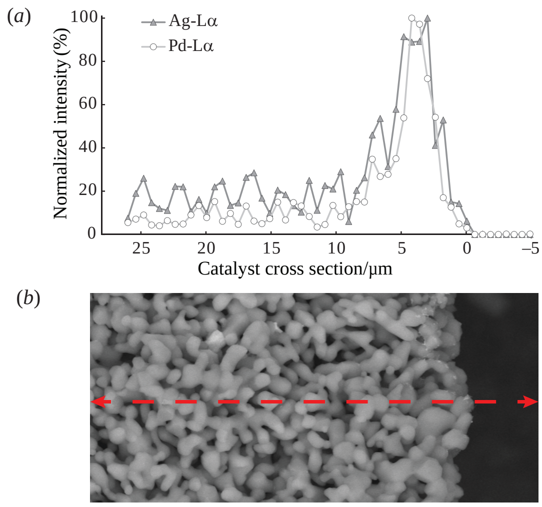

Figure 1 FESEM-EDS study of the Pd_1Ag catalyst to prove egg-shell distribution of the active component: (*a*) EDS-line scan along a red line in (*b*) the FESEM image of a PdAg pellet cross section.

scan along a red line in the FESEM image of a PdAg pellet cross section (layer from the surface to a depth of 25 μm). Signals of Pd-Lα and Ag-Lα specific X-ray lines changed in parallel to indicate that both metals were deposited within a near-surface region of an alumina granule in the close vicinity to each other. The EDS signal intensities were significantly higher in a shell layer of 8 μm than those in the inner layer due to the formation of egg-shell bimetallic catalysts.

The egg-shell structure was confirmed by X-ray photoelectron spectroscopy (Figure 2). The spectra were recorded from the outer surface of intact catalyst pellets, clearly showing that Pd and Ag were concentrated in the outer layer. The surface Pd/Al atomic ratios determined by XPS were 2.83×10^{-2} and 5.68×10^{-2} for Pd and Pd_1Ag samples, respectively; they are about two orders of magnitude higher than the value for a bulk composition (3.83×10^{-4}, Table S1). Note that, if the catalyst granules were destroyed and XPS spectra were taken from the obtained powder, the intensity of the Pd3*d* and Ag3*d* signals became below the instrumental detection limit. This fact shows that the main portion of Pd was concentrated in the shell of a catalyst granule.

The XPS spectra also confirmed the PdAg alloy formation. Figure 2 shows the Pd3*d* spectra of the Pd and PdAg samples. The $Pd3d_{5/2}$ component with a binding energy of 335.1 eV was attributed to metallic palladium in the Pd catalyst. The binding energy of the $Pd3d_{5/2}$ peak for the bimetallic PdAg catalyst was 334.8 eV, that is, shifted by 0.3 eV to lower energy with respect to that in the monometallic Pd sample. According to published data,[24–26] this typical shift indicates the formation of bimetallic PdAg alloyed nanoparticles by electron transfer from Ag to Pd. The calculated Ag : Pd surface atomic ratio (~3.1) is above the nominal 2 : 1 stoichiometry of the $PdAg_2$ catalyst due to the surface enrichment of PdAg nanoparticles in Ag. This is typical for Pd–Ag alloy nanoparticles[27,28] and consistent with the results of theoretical calculations indicating Ag surface segregation due to the formation of a more thermodynamically stable system.[29,30]

The Pd_1Ag SAA structure formation was evidenced by DRIFT spectra of adsorbed CO after *in situ* oxidative–reductive treatment (Figure 3). The DRIFT CO spectrum of the monometallic Pd catalyst exhibited an intense broad absorption band at 1985 cm^{-1} with a shoulder at ~1940 cm^{-1}. This peak was attributed to bridged CO on multiatomic Pd_n sites, while the shoulder was due to bridged CO adsorbed on large planes of palladium nanoparticles.[31] A symmetric absorption band at 2094 cm^{-1} was attributed to CO linearly adsorbed on Pd(111) faces or surface defect sites (edges, corners, *etc*.).[32]

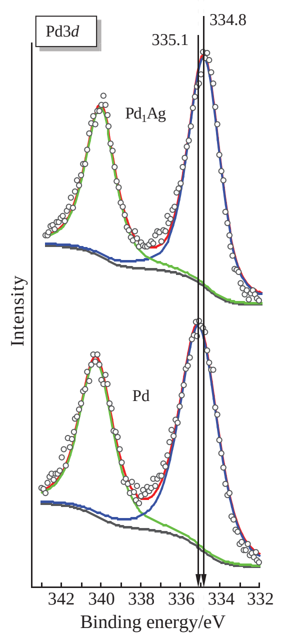

Figure 2 Pd3*d* XPS spectra of Pd_1Ag and reference Pd egg-shell catalysts.

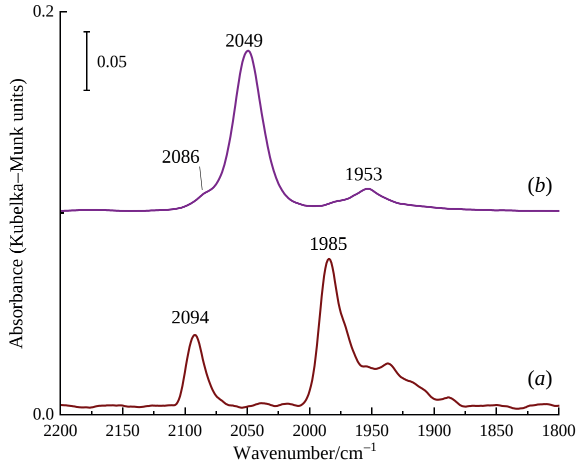

Figure 3 Normalized DRIFT spectra of CO adsorbed on (*a*) monometallic Pd and (*b*) Pd_1Ag catalysts.

The spectrum of the *in situ* freshly reduced bimetallic Pd_1Ag catalyst showed intense signal at 2049 cm^{-1} assigned to CO molecules linearly adsorbed on the top of Pd atoms surrounded by Ag atoms. The absorption band maximum was shifted by 45 cm^{-1} towards lower wavenumbers as a result of electronic interaction between palladium and silver due to the formation of a solid solution. The bathochromic shift can be explained by the absence of dipole–dipole interaction between adsorbed CO molecules and the electronic effects induced by silver. A weak shoulder at 2086 cm^{-1} was assigned to linear CO adsorbed on the bimetallic Pd–Ag particles depleted with Ag. A small peak at 1960–1950 cm^{-1} was ascribed to bridged CO on Pd_2 sites. This peak resulted from the formation of an insignificant amount of Ag-depleted PdAg particles after the decomposition of the $PdAg_2(OAc)_4(HOAc)_4$ complex upon reductive treatment. An extremely low intensity of this signal indicates an almost complete absence of multiatomic Pd_n ($n \geqslant 2$) sites in the egg-shell catalyst and the predominance of Pd_1 sites isolated by Ag.[13–15]

The catalytic performances of Pd_1Ag and reference monometallic Pd samples were compared in selective acetylene hydrogenation. Note that all catalysts were treated in an air flow (500 °C, 90 min) and then in a flow of 5 wt% H_2/Ar (500 °C, 1.5 h) before catalytic tests. In these comparative tests, the catalyst loads were 150 and 300 mg for the Pd and Pd_1Ag samples, respectively. Figure 4(*a*) shows the temperature dependence of C_2H_2 conversion. Since the activity of Pd_1Ag SAA is slightly lower than that of the monometallic Pd sample, the loaded catalyst amounts were adjusted to obtain identical acetylene conversion–reaction temperature dependences. Therefore, the selectivities were compared at identical acetylene conversion and temperature. For better comparability, the catalyst activity was normalized by the amount of Pd (Table S2). The catalytic activity of Pd_1Ag decreased by a factor of 1.7 from 0.071 to 0.042 $mmol_{C_2H_2}^{-1}$ mg_{Pd}^{-1} min^{-1} compared to the Pd counterpart.

Note that Ag significantly improved the selectivity for ethylene, especially at high acetylene conversions. At low acetylene conversions, selectivity reached ~96 and ~93% on Pd_1Ag and Pd, respectively, and remained almost constant up to an acetylene conversion of 60%. As the acetylene conversion increased, the selectivity rapidly dropped to ~60% at a C_2H_2 conversion of 90% on monometallic Pd. On the other hand, the selectivity of the Pd_1Ag SAA catalyst for ethylene was as high as 90.2%. Presumably, this catalytic behavior was due to the predominance of Pd_1 single-atom sites isolated from each other

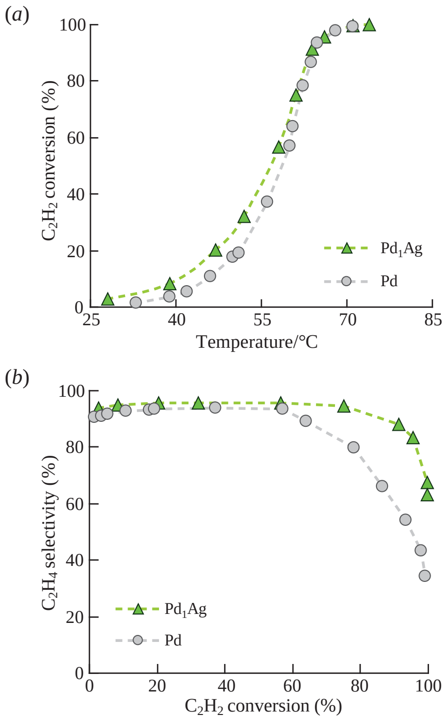

Figure 4 Catalytic performance of Pd_1Ag SAA and reference Pd egg-shell catalysts in acetylene hydrogenation: (*a*) the temperature dependence of C_2H_2 conversion and (*b*) the selectivity for C_2H_4 as a function of C_2H_2 conversion. Catalysts loadings: Pd_1Ag, 300 mg and Pd, 150 mg.

by Ag atoms and the absence of multiatomic Pd_n ensembles ($n \geqslant 2$), as evidenced by DRIFT CO. The structure of active sites allowed ethylene adsorption only as weakly π-bonded species, thus facilitating ethylene desorption and improving the catalyst selectivity for ethylene.

Thus, the use of the $PdAg_2(OAc)_4(HOAc)_4$ complex as a precursor allowed us to prepare Pd_1Ag catalysts with an egg-shell distribution of the active component, which was evidenced by FESEM-EDS data. The formation of a PdAg alloy was verified by XPS analysis. According to DRIFTS-CO results, the structure of active sites corresponded to the single-atom alloy. In acetylene hydrogenation, the Pd_1Ag/Al_2O_3 egg-shell catalyst exhibited excellent selectivity for ethylene formation, and it can be considered as a promising catalytic system for practical implementation.

This work was supported by the Russian Science Foundation (grant no. 23-13-00301; https://rscf.ru/en/project/23-13-00301).

We are grateful to Prof. M. N. Vargaftik and Dr. I. A. Yakushev (N. S. Kurnakov Institute of General and Inorganic Chemistry, RAS) for supplying us with the $PdAg_2(OAc)_4(HOAc)_4$ complex. Electron microscopy characterization was performed at the Department of Structural Studies of Zelinsky Institute of Organic Chemistry, RAS. XPS analysis was performed by Dr. A. A. Sadovnikov using the equipment of the Shared Research Center ‘Analytical Center of Deep Oil Processing and Petrochemistry of TIPS RAS’.

Online Supplementary Materials

Supplementary data associated with this article can be found in the online version at doi: 10.1016/j.mencom.2023.10.032.

References

1 T. D. Shittu and O. B. Ayodele, *Front. Chem. Sci. Eng*., 2022, **16**, 1031.
2 M. Takht Ravanchi, S. Sahebdelfar and S. Komeili, *Rev. Chem. Eng*., 2018, **34**, 215.
3 A. J. McCue and J. A. Anderson, *Front. Chem. Sci. Eng*., 2015, **9**, 142.
4 A. Borodziński and G. C. Bond, *Catal. Rev*., 2006, **48**, 91.
5 A. Borodziński and G. C. Bond, *Catal. Rev*., 2008, **50**, 379.
6 R. T. Hannagan, G. Giannakakis, M. Flytzani-Stephanopoulos and E. C. H. Sykes, *Chem. Rev*., 2020, **120**, 12044.
7 G. Giannakakis, M. Flytzani-Stephanopoulos and E. C. H. Sykes, *Acc. Chem. Res*., 2019, **52**, 237.
8 T. Zhang, A. G. Walsh, J. Yu and P. Zhang, *Chem. Soc. Rev*., 2021, **50**, 569.
9 G. Kyriakou, M. B. Boucher, A. D. Jewell, E. A. Lewis, T. J. Lawton, A. E. Baber, H. L. Tierney, M. Flytzani-Stephanopoulos and E. C. H. Sykes, *Science*, 2012, **335**, 1209.
10 S. Chai, D. Gao, J. Xia, Y. Yang and X. Wang, *ChemCatChem*, 2023, **15**, e202300217.
11 J. Wang, H. Xu, C. Che, J. Zhu and D. Cheng, *ACS Catal*., 2023, **13**, 433.
12 L. Jiang, K. Liu, S.-F. Hung, L. Zhou, R. Qin, Q. Zhang, P. Liu, L. Gu, H. M. Chen, G. Fu and N. Zheng, *Nat. Nanotechnol*., 2020, **15**, 848.
13 G. X. Pei, X. Y. Liu, A. Wang, A. F. Lee, M. A. Isaacs, L. Li, X. Pan, X. Yang, X. Wang, Z. Tai, K. Wilson and T. Zhang, *ACS Catal*., 2015, **5**, 3717.
14 A. V. Rassolov, I. S. Mashkovsky, G. O. Bragina, G. N. Baeva, P. V. Markov, N. S. Smirnova, J. Wärnå, A. Yu. Stakheev and D. Yu. Murzin, *Mol. Catal*., 2021, **506**, 111550.
15 N. S. Smirnova, G. N. Baeva, P. V. Markov, I. S. Mashkovsky, A. V. Bukhtiyarov, Y. V. Zubavichus and A. Yu. Stakheev, *Mendeleev Commun*., 2022, **32**, 807.
16 M. Kuhn, M. Lucas and P. Claus, *Catal. Commun*., 2015, **72**, 170.
17 M. Kuhn, M. Lucas and P. Claus, *Chem. Eng. Technol*., 2015, **38**, 61.
18 M. Kuhn, M. Lucas and P. Claus, *Ind. Eng. Chem. Res*., 2015, **54**, 6683.
19 M. Takht Ravanchi and S. Sahebdelfar, *Appl. Catal., A*, 2016, **525**, 197.
20 M. Takht Ravanchi, S. Sahebdelfar, M. Rahimi Fard and H. Moosavi, *Iran. J. Chem. Eng*., 2021, **18**, 19.
21 A. Pachulski, R. Schödel and P. Claus, *Appl. Catal., A*, 2011, **400**, 14.
22 N. Yu. Kozitsyna, S. E. Nefedov, A. P. Klyagina, A. A. Markov, Zh. V. Dobrokhotova, Yu. A. Velikodny, D. I. Kochubey, T. S. Zyubina, A. E. Gekhman, M. N. Vargaftik and I. I. Moiseev, *Inorg. Chim. Acta*, 2011, **370**, 382.
23 A. V. Rassolov, D. S. Krivoruchenko, M. G. Medvedev, I. S. Mashkovsky, A. Yu. Stakheev and I. V. Svitanko, *Mendeleev Commun*., 2017, **27**, 615.
24 D. V. Glyzdova, T. N. Afonasenko, E. V. Khramov, N. N. Leont’eva, I. P. Prosvirin, A. V. Bukhtiyarov and D. A. Shlyapin, *Appl. Catal., A*, 2020, **600**, 117627.
25 M. A. Panafidin, A. V. Bukhtiyarov, I. P. Prosvirin, I. A. Chetyrin and V. I. Bukhtiyarov, *Kinet. Catal*., 2018, **59**, 776 (*Kinet. Katal*., 2018, **59**, 739).
26 R. N. Lamb, B. Ngamsom, D. L. Trimm, B. Gong, P. L. Silveston and P. Praserthdam, *Appl. Catal., A*, 2004, **268**, 43.
27 A. V. Rassolov, P. V. Markov, G. O. Bragina, G. N. Baeva, D. S. Krivoruchenko, I. S. Mashkovskii, I. A. Yakushev, M. N. Vargaftik and A. Yu. Stakheev, *Kinet. Catal*., 2016, **57**, 859 (*Kinet. Katal*., 2016, **57**, 857).
28 P. T. Wouda, M. Schmid, B. E. Nieuwenhuys and P. Varga, *Surf. Sci*., 1998, **417**, 292.
29 M. Ropo, *Phys. Rev. B*, 2006, **74**, 195401.
30 O. M. Lovvik, *Surf. Sci*., 2005, **583**, 100.
31 S. K. Kim, C. Kim, J. H. Lee, J. Kim, H. Lee and S. H. Moon, *J. Catal*., 2013, **306**, 146.
32 G. Agostini, R. Pellegrini, G. Leofanti, L. Bertinetti, S. Bertarione, E. Groppo, A. Zecchina and C. Lamberti, *J. Phys. Chem. C*, 2009, **113**, 10485.

Received: 5th June 2023; Com. 23/7184